Polymer 78 (2015) 69–80

Contents lists available at ScienceDirect

Polymer

journal homepage: www.elsevier.com/locate/polymer

Supramolecular assembly of diblock copolymer blends with hydrogen-bonding interactions modeled by Yukawa potentials

Xu Zhang [a], Jingyuan Lin [b], Liquan Wang [a, **], Liangshun Zhang [a], Jiaping Lin [a, *], Liang Gao [a]

[a] Shanghai Key Laboratory of Advanced Polymeric Materials, State Key Laboratory of Bioreactor Engineering, Key Laboratory for Ultrafine Materials of Ministry of Education, School of Materials Science and Engineering, East China University of Science and Technology, Shanghai 200237, China
[b] School of Marine Science, Shanghai Ocean University, Shanghai 201306, China

ARTICLE INFO

Article history:
Received 11 June 2015
Received in revised form
4 September 2015
Accepted 26 September 2015
Available online 30 September 2015

Keywords:
Assembly
Hydrogen bond
Self-consistent field theory

ABSTRACT

We extended self-consistent field theory to study the phase behavior of supramolecular blends of diblock copolymers with hydrogen-bonding interactions. The hydrogen-bonding interactions are described by Yukawa potentials. The hydrogen-bonding donors and acceptors were modeled as two blocks smeared with opposite screened charges. Hierarchical microstructures such as parallel and perpendicular lamellae-in-lamellae were observed. The appearance of parallel/perpendicular lamellae-in-lamellae depends on the strength of hydrogen-bonding interactions related to the density of hydrogen bonds and the characteristic lengths of the Yukawa potentials. Phase diagrams were correspondingly mapped out, and the domain size, interfacial width and free energies were examined to gain insight into the phase transitions. It was also found that the revealed mechanism can account for some experimental phenomena that are not well explained yet. The present method can be readily further extended to more complicated supramolecular systems with hydrogen-bonding interactions.

1. Introduction

Supramolecular polymers are kinds of materials which utilize non-covalent bonding interactions such as hydrogen-bonding interactions and electrostatic interactions to connect chemically dissimilar polymers into a dynamic molecular architecture [1–5]. The introduction of non-covalent bonding interactions into polymer blend systems would effectively suppress the macrophase separation. In the supramolecular polymers, the mixing blocks with varying ratios offer a straightforward and efficient way to generate a series of microstructures, without having to synthesize complicated copolymers. Moreover, the supramolecular polymers would offer a great platform for fabricating materials with highly tunable properties, such as environmental adaptation and self-repair capacity, owning to the temperature/pH-dependence of the non-covalent interactions [6,7].

Inspired by the ability of supramolecular polymers to adjust the versatilities and response to environments, plenty of efforts have been made to understand the phase behaviors of supramolecular polymers [8–16]. A widely-studied system is the blends of AB- and B'C-diblock copolymers with B- and B'-blocks miscible by hydrogen-bonding interactions. Matsushita et al. prepared blends of polyisoprene-*b*-poly(2-vinylpyridine) (PI-*b*-P2VP) and poly(4-hydroxystyrene)-*b*-polystyrene (P4HS-*b*-PS) diblock copolymers, where the hydrogen bonds can be formed between the P2VP- and P4HS-blocks [8]. The change of the molar ratio and the symmetry of diblock copolymers can lead to a variety of hierarchical microstructures such as perpendicular lamellae-in-lamellae and spheres-in-lamellae. Fredrickson et al. designed a mixture of poly(ethylene oxide)-*b*-poly(styrene-*r*-4-hydroxystyrene) (PEO-*b*-PS4HS) and poly(styrene-*r*-4-vinylpyridine)-*b*-poly(methyl methacrylate) (PS4VP-*b*-PMMA) with various fractions of hydrogen-bonded phenolic and pyridyl units [9,10]. The effect of the hydrogen-bonding strengths on the hierarchical microstructures was examined by controlling over the relative densities of hydrogen-bonding donors and acceptors. It was found that hierarchical square arranged nanostructures and hexagonally packed microstructures are formed at different ratios of donors to acceptors.

In addition to the experiments, theory and simulations were

* Corresponding author.
** Corresponding author.
E-mail addresses: lq_wang@ecust.edu.cn (L. Wang), jlin@ecust.edu.cn (J. Lin).

http://dx.doi.org/10.1016/j.polymer.2015.09.065
0032-3861/

utilized to study the phase behavior of the supramolecular polymers [17–20]. One powerful theory successful in accounting for general phase behaviors of complex polymeric systems is self-consistent field theory (SCFT) [21–36]. It has been applied to supramolecular polymers with hydrogen-bonding interactions [37–41]. Recently, there are two approaches for tackling the hydrogen-bonding interactions in the framework of SCFT. One of the methods is to use a negative Flory–Huggins parameter to account for the hydrogen-bonding interactions. Fredrickson et al. developed this method to examine the self-assembly of AB/B'C diblock copolymer blends. An agreement with the experimental observations proves that this method is sufficient to understand qualitative aspects of the self-assembly of supramolecular systems [9,10]. However, it is unphysical to treat the hydrogen-bonding interactions with a negative Flory–Huggins parameter. This is because that the hydrogen-bonding donors and acceptors are chemically incompatible ($\chi N > 0$) although they are attracted each other. Another method is to treat hydrogen-bonding donors and acceptors as chemically reactive polymers with hetero-complementary bonding groups [37–41]. In this method, the immiscibility between chemically different polymers are still described by Flory–Huggins parameters. The drawback of this method is that it suffers from difficulties in studying the systems with multiple hydrogen bonds. This is due to the fact that the computational cost dramatically increases with increasing the number of hydrogen bonds. (Note that the supramolecular systems generally contain a large number of hydrogen bonds in each block.) To overcome the drawbacks of these two methods, new SCFT method should be developed for the supramolecular copolymers.

In this work, we assumed the hydrogen-bonding interactions as electrostatic dipole–dipole interactions. The dipole–dipole interactions are implicitly described by Yukawa potentials which is also named screened Coulomb potentials [42,43]. Based on this assumption, a SCFT coupled with the screened Poisson equation can be derived. This method was first developed by Nogovitsin et al. for investigating the behavior of polyelectrolyte chains in aqueous salt solutions [44]. We extended this method to a different polymer system, namely, supramolecular blends of diblock copolymers with hydrogen-bonding interactions. The hydrogen-bonding donors and acceptors are modeled as two charged blocks smeared with opposite screened charges. Such an approach can overcome the deficiencies of two commonly used methods — may rationally describe the immiscibility between different polymers and could be suit for multiple-hydrogen-bond supramolecular systems [42,43]. Furthermore, the method can bridge a gap between the hydrogen-bonding interactions and electrostatic interactions by varying the parameters in Yukawa potential. Then, we applied this method to study the supramolecular blends of AB- and B'C-diblock copolymers where B- and B'-blocks can be associated with the hydrogen bonds. The effect of the density of hydrogen bonds and two characteristic lengths of the Yukawa potential on the phase behaviors were examined. It was found that the parallel-to-perpendicular lamellae-in-lamella transition occurs by varying these parameters. Based on the obtained data, phase diagrams were mapped out. This work provides reasonable information about the phase behavior of supramolecular copolymers, and the SCFT method can be readily extended to more complicated supramolecular systems.

2. Theoretical method

A system of volume V consisting of n_{AB} AB-diblock copolymers and $n_{B'C}$ B'C-diblock copolymers was considered. The incompressibility condition constrains the bulk density of segment number to a constant value ρ_0 at each point in the space. The block copolymers are assumed to be monodisperse with the same statistical segment length a. The total statistical segment of P-diblock copolymers (P = AB and B'C) is N_P, where $N_{AB} = N$ and $N_{B'C} = \alpha_{B'C}N$ for AB- and B'C-diblock copolymers, respectively. Here, $\alpha_P = N_P/N$ is the length ratio of P-diblock copolymer to AB-diblock copolymer. For AB-diblock copolymers, the volume fraction of A- and B-blocks is f_A and f_B, respectively. Similarly, for B'C-diblock copolymers, the volume fraction of B'- and C-block is $f_{B'}$ and f_C, respectively. Thus, $f_A + f_B = 1$ and $f_{B'} + f_C = 1$. In the supramolecular system, one block can be connected with another block through hydrogen bonds. The two kinds of blocks attracted by hydrogen bonds were smeared with opposite screened charges. The valence number of these blocks is denoted as z_I (I = A, B, B′, and C), and the corresponding charge is $z_I e$ (e is the elementary charge).

The partition function of this supramolecular system is given by

$$Z = \prod_P \left(\frac{\zeta_P^{n_P}}{n_P!} \prod_{k=1}^{n_P} \int D\mathbf{R}_{k,P} \right) \times \int D\psi \prod_P \prod_k^{n_P} \times \sum_{\theta_{k,P}(s)} \exp\left(-\frac{H}{k_B T} \right) \delta \left[\int d\mathbf{r} \hat{\phi}_e(\mathbf{r}) \right] \prod_{\mathbf{r}} \delta \left[\sum_I \hat{\phi}_I(\mathbf{r}) - 1 \right] \tag{1}$$

Here, ζ_P is the partition function of a single chain due to the kinetic energy; n_P is the number of P-diblock copolymer; $\mathbf{R}_{k,P}$ is the space curve of the kth P-polymer chain; ψ is the electrostatic potential at $\mathbf{r}$ position. $\theta_{k,P}(s)$ denotes the charge density of the sth segment of kth chain of P-diblock copolymer. $\sum_{\theta_{k,P}(s)}$ is a summation over the charge distributions of the kth chain of P-diblock copolymer. The Hamiltonian H of the system consists of three parts

$$H = H_0 + H_1 + H_2 \tag{2}$$

where

$$H_0 = \frac{3k_B T}{2a^2} \sum_P \sum_{k=1}^{n_P} \int_0^{N_P} ds \left| \frac{d\mathbf{R}_k(s)}{ds} \right| \tag{3}$$

is the elastic energy of Gaussian chains. The k_B and T is the Boltzmann constant and temperature, respectively.

$$H_1 = \frac{\rho_0 k_B T}{2} \sum_{\substack{I,J \\ I \neq J}} \int d\mathbf{r} \chi_{IJ} \hat{\phi}_I(\mathbf{r}) \hat{\phi}_J(\mathbf{r}) \tag{4}$$

describes the short-range interaction energy of the system, where χ_{IJ} is the Flory–Huggins interaction parameter between I- and J-species (in unit of $k_B T$). The local microscopic densities of different species at the position $\mathbf{r}$ are defined by

$$\hat{\phi}_I(\mathbf{r}) = \frac{1}{\rho_0} \sum_P \sum_{k=1}^{n_P} \int_0^{N_P} ds \sigma_{I,P}(s) \delta[\mathbf{r} - \mathbf{R}_{k,P}(s)] \tag{5}$$

Here, $\sigma_{I,P}(s) = 1$ (or 0) represents that the sth segment of P-diblock polymers is of type I (or not). The hydrogen bond is usually described as an electrostatic dipole–dipole interaction. To mimic correlation effect between dipoles in a way compatible with the self-consistent field theory, we add a field $\psi(\mathbf{r})$ to the energy of a dipole (donor/acceptor) at position $\mathbf{r}$ [44,45]. The Yukawa potential has been used to describe the interaction between dipoles (*e.g.* water) implicitly, and found that it can successfully account for the correlation effects between dipoles [42,43]. The electrostatic energy of the system is given by

$$H_2 = \int d\mathbf{r}d\mathbf{r}'\widehat{\phi}_e(\mathbf{r})\psi(\mathbf{r}-\mathbf{r}')\widehat{\phi}_e(\mathbf{r}') \tag{6}$$

where the microscopic densities of the screened charges are

$$\widehat{\phi}_e(\mathbf{r}) = \sum_P \sum_{k=1}^{n_P} \int_0^{N_P} ds\theta_{k,P}(s)z_P(s)e\delta\left[\mathbf{r}-\mathbf{R}_{k,P}(s)\right] \tag{7}$$

where $\psi(\mathbf{r})$ is derived from a Yukawa potential. The Yukawa potential is

$$\psi(\mathbf{r}) = -\eta\frac{e^{-\lambda|\mathbf{r}|}}{|\mathbf{r}|} = -\eta\int\frac{4\pi}{\mathbf{k}^2+\lambda^2}e^{i\mathbf{k}\mathbf{r}}d\mathbf{k} \tag{8}$$

where η and λ are the two characteristic lengths of the Yukawa potential. The η is the amplitude of potential related to the dielectric permittivity and the λ is the screening length that determines the range of the potential. The Yukawa potential is set to be attractive in order to account for hydrogen-bonding interactions between various blocks. This type of potential was previously used to account for the interaction of hyaluronic acid chains in salt solutions [44]. To decouple the interaction in Eq. (6), the identity (8) and Hubbard–Stratonovich transformation were used. The electrostatic energy then becomes

$$H_2 = \int d\mathbf{r}\widehat{\phi}_e(\mathbf{r})\psi(\mathbf{r}) - \int d\mathbf{r}\frac{1}{8\pi\eta}\left(|\nabla\psi(\mathbf{r})|^2+\lambda^2\psi(\mathbf{r})^2\right) \tag{9}$$

Subsequently integral representations for the delta functions are inserted into the partition function (Eq. (1)). We use the following integral representations,

$$\delta\left[\phi_I(\mathbf{r})-\widehat{\phi}_I(\mathbf{r})\right] = \int d\omega_I \exp\left\{\int d\mathbf{r}\rho_0\omega_I(\mathbf{r})\left[\phi_I(\mathbf{r})-\widehat{\phi}_I(\mathbf{r})\right]\right\} \tag{10}$$

$$\delta\left[\sum_I\phi_I(\mathbf{r})-1\right] = \int d\xi \exp\left\{\int d\mathbf{r}\rho_0\xi(\mathbf{r})\left[\sum_I\phi_I(\mathbf{r})-1\right]\right\} \tag{11}$$

it introduces a density field $\phi_I(\mathbf{r})$ constrained to $\widehat{\phi}_I(\mathbf{r})$ and an effective chemical potential field $\omega_I(\mathbf{r})$ conjugated to the density fields. The Lagrange multiplier $\xi(\mathbf{r})$ is introduced to enforce the incompressibility constraint ($\sum\phi_I(\mathbf{r}) = 1$). The partition function (eq. (1)) becomes

$$Z = \int\prod_I(D\phi_I D\omega_I)D\psi D\xi \exp\left(-\frac{F}{k_BT}\right) \tag{12}$$

where F is the free energy of the system, written as

$$\frac{NF}{\rho_0 V k_BT} = \frac{N}{V}\int d\mathbf{r}\left\{\frac{1}{2}\sum_{\substack{I,J\\I\neq J}}\chi_{IJ}\phi_I(\mathbf{r})\phi_J(\mathbf{r}) - \sum_I\omega_I(\mathbf{r})\phi_I(\mathbf{r}) - \frac{k_BT}{8\pi\rho_0\eta}\left[|\nabla\varphi(\mathbf{r})|^2+\lambda^2\varphi(\mathbf{r})^2\right] - \xi(\mathbf{r})\left[1-\sum_I\phi_I(\mathbf{r})\right]\right\} - \sum_P\frac{c_P}{\alpha_P}\ln\left(\frac{Q_P}{V}\right) \tag{13}$$

Here, $c_P = n_P N/\rho_0 V$ is the volume-averaged fraction of P-diblock copolymers and $\varphi(\mathbf{r}) = \psi(\mathbf{r})/k_BT$. Q_P is the single chain partition function for the P-diblock copolymers, given by

$$Q_P = \frac{\int D\mathbf{R}exp\left\{-\int_0^{N_P}ds\left[\frac{3}{2a^2}\left|\frac{d\mathbf{R}(s)}{ds}\right|^2+\omega(\mathbf{R}(s))+\theta_P(s)z_P(s)e\varphi(\mathbf{R}(s))\right]\right\}}{\int D\mathbf{R}exp\left\{-\frac{3}{2a^2}\int_0^{N_P}ds\left|\frac{d\mathbf{R}(s)}{ds}\right|^2\right\}} \tag{14}$$

The partition function, Q_P, can be expressed in terms of propagators, $q_P(\mathbf{r},t)$, which are written as $Q_P = \int d\mathbf{r}q_P(\mathbf{r},1)$. The contour length t starts from one end of the polymer chain ($t = 0$) to the other ($t = 1$). The spatial coordinate $\mathbf{r}$ is rescaled by R_g, where $R_g^2 = Na^2/6$. The propagator $q_P(\mathbf{r},t)$ represents the probability of finding segments t at position $\mathbf{r}$, which satisfies the following modified diffusion equations

$$\frac{\partial q_P(\mathbf{r},t)}{\partial t} = \nabla^2 q_P(\mathbf{r},t) - N\sum_I\left\{[\omega_I(\mathbf{r})+\theta_I z_I\varphi(\mathbf{r})]\sigma_{I,P}(t\alpha_P N)\right\}q_P(\mathbf{r},t) \tag{15}$$

subject to the initial condition $q_P(\mathbf{r},0) = 1$. The backward propagators $q_P^*(\mathbf{r},t)$ satisfy the following modified diffusion equations

$$\frac{\partial q_P^*(\mathbf{r},t)}{\partial t} = \nabla^2 q_P^*(\mathbf{r},t) - N\sum_I\left\{[\omega_I(\mathbf{r})+\theta_I z_I\varphi(\mathbf{r})]\sigma_{I,P}(t\alpha_P N)\right\}q_P^*(\mathbf{r},t) \tag{16}$$

subject to the initial condition $q_P^*(\mathbf{r},0) = 1$.

The mean-field equations are obtained by the saddle-point approximation, setting $\delta F/\delta\phi_I = 0$, $\delta F/\delta\omega_I = 0$, and $\delta F/\delta\xi = 0$. The SCFT equations can be written as

$$\omega_I(\mathbf{r}) = \sum_{\substack{I,J=A,B,B',C\\I\neq J}}\chi_{IJ}\phi_J(\mathbf{r}) + \xi(\mathbf{r}) \tag{17}$$

$$\phi_I(\mathbf{r}) = \sum_{P=AB,B'C}\frac{c_P V}{\alpha_P N Q_P}\int_0^1 q_P(\mathbf{r},t)q_P^*(\mathbf{r},1-t)\sigma_{I,P}(t\alpha_P N)dt \tag{18}$$

$$\sum_{I=A,B,B',C}\phi_I(\mathbf{r}) = 1 \tag{19}$$

The electrostatic potential is determined by a screened Poisson equation, which is obtained by minimizing the free energy with respect to the electrostatic potential, *i.e.* $\delta F/\delta\varphi = 0$, which is given as

$$\left(\nabla^2 - \lambda^2\right)\varphi(\mathbf{r}) = -\frac{\phi_e(\mathbf{r})}{\gamma} \tag{20}$$

where the constant $\gamma = 1/8\pi\eta$. $\phi_e(\mathbf{r})$ is a summation over the charge densities at position $\mathbf{r}$, which is written as

$$\phi_e(\mathbf{r}) = \sum_I z_I\theta_I\phi_I(\mathbf{r}) \tag{21}$$

One of the main tasks is to solve the screened Poisson equation. This equation was solved with spectral method, whose computational cost is much smaller than that of solving diffusion equations (15) and (16). Therefore, the computational cost does not increase too much. Moreover, the cost is independent of the number of hydrogen bonds, and thereby the method suits for multiple-hydrogen-bond systems. The detailed spectral method is given as

$$\varphi(\mathbf{r}) = \mathrm{F}^{-1}\left(-\frac{1}{k^2+\lambda^2}\cdot\mathrm{F}\left(-\frac{\phi_e(\mathbf{r})}{\gamma}\right)\right) \tag{22}$$

where F and F^{-1} represent forward and inverse Fourier transform operations, respectively.

The free energy can be split into the contributions of enthalpy U and entropy S, *i.e.*, $F = U - TS$, where $U = U_\chi + U_e$. These terms possess the following expressions:

$$\frac{NU_\chi}{\rho_0 V k_B T} = \frac{N}{2V}\int d\mathbf{r}\sum_{\substack{I,J\\ I\neq J}}\chi_{IJ}\phi_I(\mathbf{r})\phi_J(\mathbf{r}) \tag{23}$$

$$\frac{NU_e}{\rho_0 V k_B T} = \frac{N}{V}\int d\mathbf{r}\left\{\varphi(\mathbf{r})\phi_e(\mathbf{r}) - \frac{k_B T}{8\pi\rho_0\eta}\left[|\nabla\varphi(\mathbf{r})|^2 + \lambda^2\varphi(\mathbf{r})^2\right]\right\} \tag{24}$$

$$\frac{NS}{\rho_0 V k_B} = \frac{N}{V}\int d\mathbf{r}\left\{\sum_I \omega_I(\mathbf{r})\phi_I(\mathbf{r}) + \varphi(\mathbf{r})\phi_e(\mathbf{r})\right\} + \sum_P\frac{c_P}{\alpha_P}\ln\left(\frac{Q_P}{V}\right) \tag{25}$$

The SCFT equations were solved by using a variant of the algorithm developed by Fredrickson and co-workers [45–48]. Initial field configurations started from a general random state. The diffusion equations were solved *via* the pseudo-spectral method and operator splitting formula scheme, where the fast Fourier transforms were performed by the software package developed at MIT [49]. All of the simulations in the present work were carried out with periodic boundary conditions. Each calculation utilized a step size of $\Delta t = 0.01$ and the spatial resolution $\Delta x < 0.1R_g$. The numerical simulations proceeded until the relative accuracy in the fields (measured by $\sqrt{\sum_I\int d\mathbf{r}[\omega_I^{new}(\mathbf{r}) - \omega_I^{old}(\mathbf{r})]^2/\sum_I\int d\mathbf{r}}$) is smaller than 10^{-10} and the incompressibility condition was achieved [50,51]. The free energy was minimized with respect to the size of simulation box, as suggested by Bonbot-Raviv and Wang [52].

3. Results and discussion

The SCFT was applied to examine the phase behavior of supramolecular blends of diblock copolymers (AB/B'C) with hydrogen-bonding interactions. Such interactions are implicitly modeled by Yukawa potentials. In this work, we focused on the case that the hydrogen bonds can only occur between B- and B'-blocks, as widely studied in experiments [8–10]. As shown in Fig. 1, the B- and B'-blocks were smeared with hydrogen bonds. The interactions between them are through Yukawa potentials. Thus, we set $z_A = z_C = 0$ and $\theta_A = \theta_C = 0$. The valence number of the charges on the block is $z_B = -z_{B'} = z$. The volume fraction of the charges on the block is $\theta_B = \theta_{B'} = \theta$. For the simplicity of investigations, the AB- and B'C-diblock copolymers were treated to have the same volume-averaged fraction and equal length, *i.e.* $c_{AB} = c_{B'C} = 0.5$ and $\alpha_{AB} = \alpha_{B'C} = 1$ (or $N_{AB} = N_{B'C} = N$). The interaction strength between different blocks was set as $\chi_{AB}N = \chi_{AB'}N = \chi_{BC}N = \chi_{B'C}N = 20$ and $\chi_{AC}N = 10$, leaving $\chi_{BB'}N$ as the single alterable interaction strength. Additionally, to ensure the charge neutrality, the volume fraction of the charged B-blocks is identical to that of charged B'-blocks, parameterized by $f_A = f_C = f$ and $f_B = f_{B'} = 1\text{-}f$. Therefore, the variables in the studies are θ, λ, γ, and $\chi_{BB'}N$.

3.1. Effect of hydrogen-bonding strength on hierarchical microstructures

We first studied the microphase separation of symmetrical diblock copolymers with $f = 0.5$. Because of the symmetry of such diblock copolymers, the blends are able to form lamellar microstructures. Fig. 2 shows the hierarchical microstructures obtained from the symmetrical diblock copolymer blends with $\chi_{BB'}N = 5$, $\gamma = 0.01$, and $\lambda = 0.1$ at various values of θ. The blue, olive, green, and red colors are assigned to A-, B-, B'-, and C-blocks, respectively. Hierarchical microstructures such as parallel lamellae-in-lamellae ($\mathbf{L}^{\parallel}$, see Fig. 2a) and perpendicular lamellae-in-lamellae ($\mathbf{L}^{\perp}$, see Fig. 2b) were observed at $\theta = 0.25$ and $\theta = 0.35$, respectively. These morphologies of parallel and perpendicular lamellae-in-lamellae self-assembled from supramolecular blends of diblock copolymers have also been observed in experiments [8,53]. From Fig. 2a and b, we can see that the A-domains (blue color) and C-domains (red color) are surrounded by B-domains (olive color) and B'-domains (green color), respectively. This is due to the restriction of the covalence connected diblock copolymer architecture. More remarkable is that the B- and B'-blocks are contacted and intermixed to form BB'-domains since the attractive interactions through attractive Yukawa potentials. In addition, the two-dimensional density profile of parallel ($\mathbf{L}^{\parallel}$) and perpendicular ($\mathbf{L}^{\perp}$) hierarchical lamellae was respectively presented in Fig. 2c and d to illustrate the hierarchy of the lamellae-in-lamellae, where the black dot lines are used to emphasize the underlying order of large-length-scale and small-length-scale lamellae. As can be seen from Fig. 2c, the small-length-scale lamellae (marked by yellow arrows) are parallel to the large-length-scale lamellae (marked by light blue arrows). From Fig. 2d, it can be seen that the small-length-scale lamellae are perpendicular to the large-length-scale lamellae.

To examine the domains formed by B- and B'-blocks and get more deep insight into the hierarchical lamellae-in-lamellae, we analyzed the variation of block densities in hierarchical lamellae-in-lamellae. The one-dimensional density profiles of each block

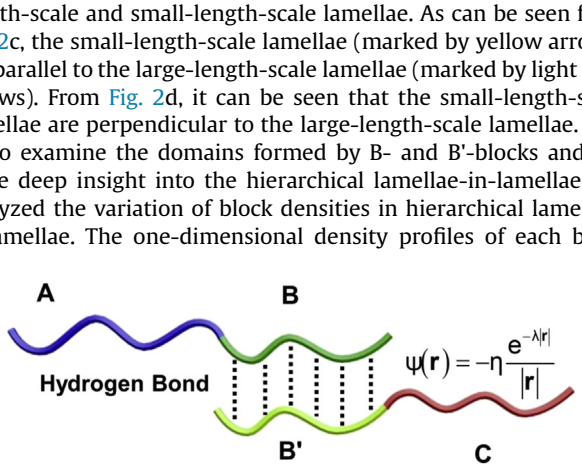

Fig. 1. Sketch of supramolecular blends of AB- and B'C-diblock copolymers. The η and λ are the two characteristic lengths of the Yukawa potential $\psi(\mathbf{r})$. The η is the amplitude of potential related to the dielectric permittivity and the λ is the screening length that determines the range of the potential.

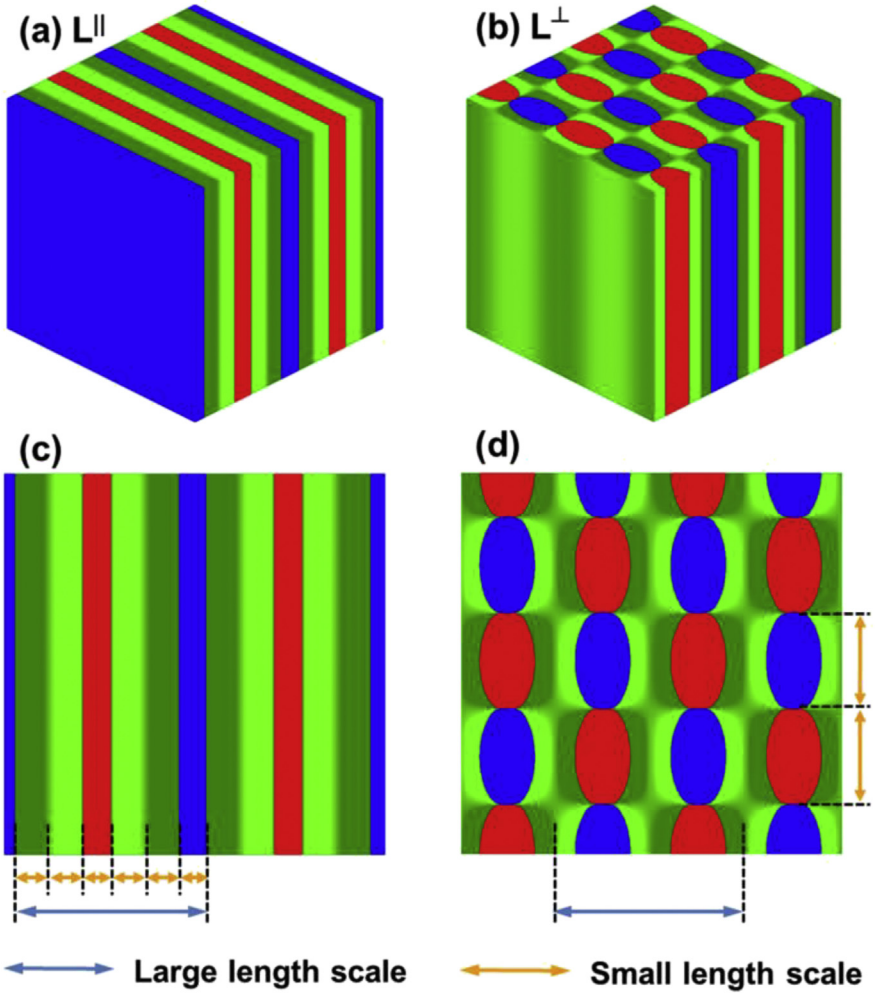

Fig. 2. (a) Parallel lamellae-in-lamellae $\mathbf{L}^{||}$ ($\theta = 0.25$) and (b) perpendicular lamellae-in-lamellae $\mathbf{L}^{\perp}$ ($\theta = 0.35$) self-assembled from the supramolecular blends of AB- and B'C-diblock copolymers with $\chi_{BB'}N = 5$, $\gamma = 0.01$, and $\lambda = 0.1$. The (c) and (d) show the corresponding cross sections of (a) and (b), respectively. The blue, olive, green, and red colors are assigned to A-, B-, B'-, and C-blocks, respectively. (For interpretation of the references to color in this figure legend, the reader is referred to the web version of this article.)

for parallel lamellae-in-lamellae $\mathbf{L}^{||}$ and perpendicular lamellae-in-lamellae $\mathbf{L}^{\perp}$ along the chosen x arrows are shown in Fig. 3. It can be seen from Fig. 3a and b that, for both the $\mathbf{L}^{||}$ and $\mathbf{L}^{\perp}$, the hydrogen-bonding donors and acceptors (B- and B'-blocks) are not homogeneously mixed but microphase-separated. The B- and B'-blocks tend to localize at the two sides of A-domains and C-domains, respectively. As shown in Fig. 3c, the A- and C-blocks contact with each other to form A/C interfaces, which further demonstrates that the microstructures are perpendicular lamellae-in-lamellae. It is due to the fact that the A/C contacts are energetically favored in terms of interfacial energy. From Fig. 3, it is noted that the degree of peak separation between ϕ_B and $\phi_{B'}$ in $\mathbf{L}^{||}$ (Fig. 3a) are stronger than that in $\mathbf{L}^{\perp}$ (Fig. 3b). This indicates that the degree of microphase separation between B- and B'-blocks in $\mathbf{L}^{||}$ are stronger than that in $\mathbf{L}^{\perp}$; namely, the B- and B'-blocks are more homogeneously mixed in $\mathbf{L}^{\perp}$ than that in $\mathbf{L}^{||}$. This would be discussed in more detail in the following sections.

We further analyzed the variation of free energies upon the formation of the observed parallel lamellae-in-lamellae $\mathbf{L}^{||}$ and perpendicular lamellae-in-lamellae $\mathbf{L}^{\perp}$. Fig. 4 shows the changes of free energy for $\mathbf{L}^{||}$ and $\mathbf{L}^{\perp}$ as a function of charge density θ, screening length λ, and inverse amplitude γ of Yukawa potential related to dielectric permittivity, respectively. As can be seen from Fig. 4a, the $\mathbf{L}^{||}$ is shown to be more stable than the $\mathbf{L}^{\perp}$ at the smaller value of θ. This indicates that the lamellae-in-lamellae can be transformed from $\mathbf{L}^{||}$ to $\mathbf{L}^{\perp}$ as the charge density increases. It can also be seen from Fig. 4a that the phase transition from $\mathbf{L}^{||}$ to $\mathbf{L}^{\perp}$ is roughly at $\theta = 0.308$ which is the intersection of the two free energy curves. In contrast to θ, the screening length λ and inverse amplitude γ of Yukawa potential play the opposite roles in determining the stability of the hierarchical lamellae-in-lamellae (see Fig. 4b and c). As the λ and γ increases, the $\mathbf{L}^{\perp}$ microstructures are transformed into the $\mathbf{L}^{||}$ microstructures. The transition points are $\lambda = 0.45$ and $\gamma = 0.013$, respectively. Because the increase in θ or decrease in λ and γ leads to an increase in the attraction between B- and B'-blocks, it implies that the perpendicular lamellae-in-lamellae $\mathbf{L}^{\perp}$ are preferred for the supramolecular blends with strong hydrogen-bonding interactions. Since the increase in θ or decrease in λ and γ play similar effect on the hydrogen-bonding interactions, we only concentrated on the influence of charge density θ in the following work.

To further clarify the dependence of the hierarchical lamellae-in-lamellae on the strength of hydrogen bonds, we calculated the domain size, the order parameter profiles, and the interfacial width for supramolecular blends with various charge densities (θ). Fig. 5 shows the lamellar period D/R_g of the hierarchical lamellae-in-lamellae as a function of θ for the supramolecular blends of AB- and B'C-diblock copolymers with $\chi_{BB'}N = 5$, $\gamma = 0.01$, and $\lambda = 0.1$. As

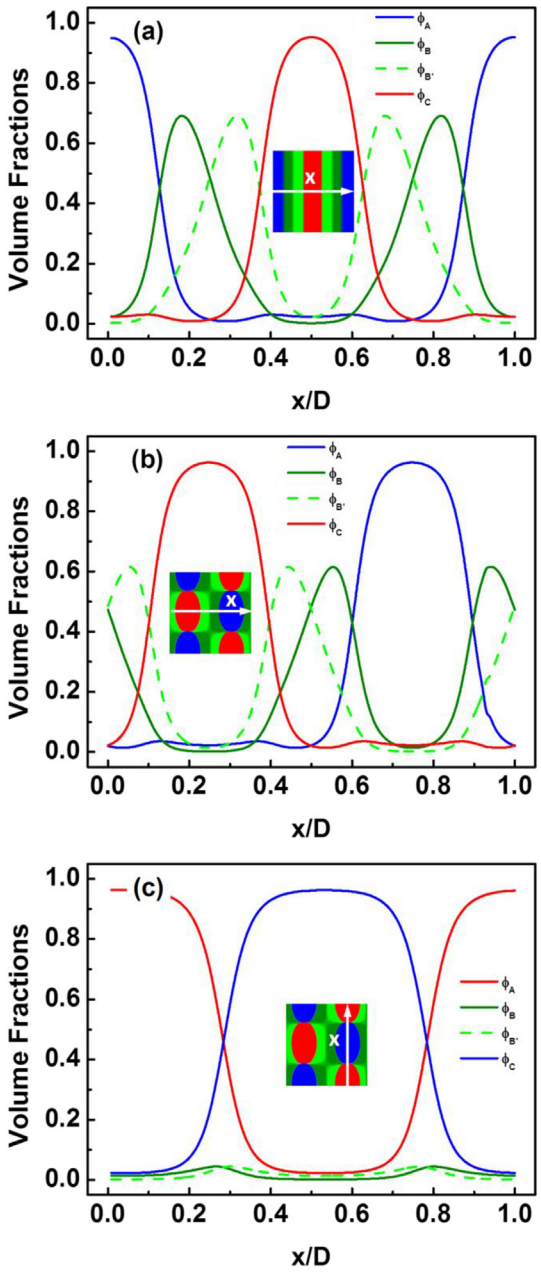

Fig. 3. One-dimensional density profiles of the blocks along the x direction of the hierarchical lamellae-in-lamellae of the supramolecular blends of AB- and B'C-diblock copolymers with $\chi_{BB'}N = 5$, $\gamma = 0.01$, and $\lambda = 0.1$ at (a) $\theta = 0.25$ and (b, c) $\theta = 0.35$. D is the lamellar period along the x direction which is indicated by white arrows in the inserts. The inserts show the cross sections, where the colors appear as same as those in Fig. 2. (For interpretation of the references to color in this figure legend, the reader is referred to the web version of this article.)

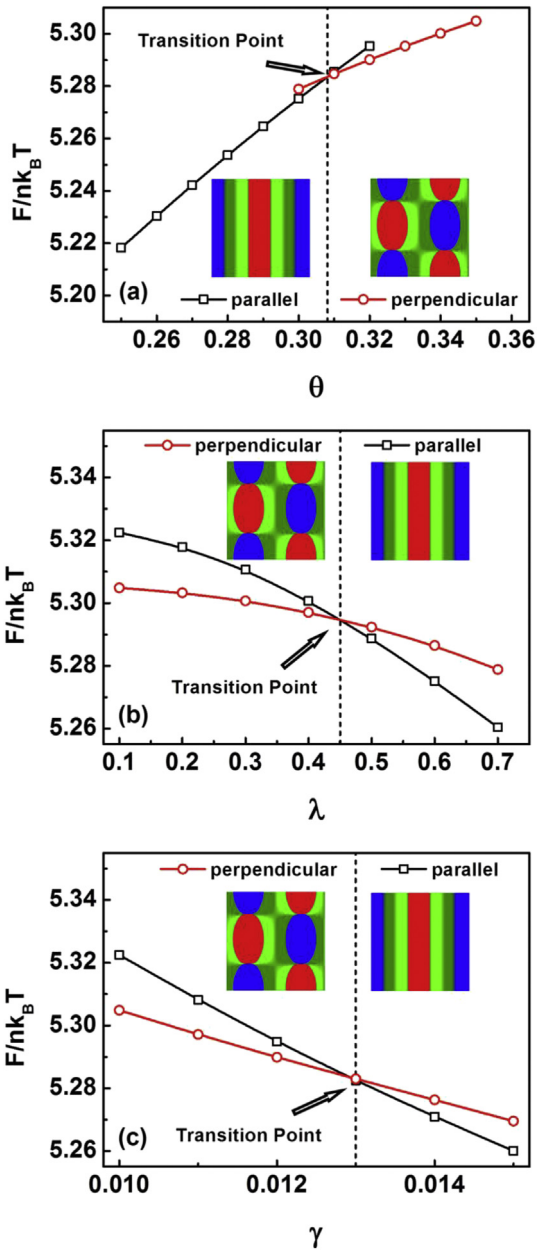

Fig. 4. Plots of free energies as a function of (a) θ at $\gamma = 0.01$ and $\lambda = 0.1$, (b) λ at $\gamma = 0.01$ and $\theta = 0.35$, and (c) λ at $\gamma = 0.01$ and $\theta = 0.35$ for the supramolecular blends of AB- and B'C-diblock copolymers with $\chi_{BB'}N = 5$ ($n = \rho_0 V/N$). The transition point between $\mathbf{L}^{||}$ and $\mathbf{L}^{\perp}$ is indicated by an arrow. The inserts show two-dimensional density profiles of parallel lamellae-in-lamellae $\mathbf{L}^{||}$ and perpendicular lamellae-in-lamellae $\mathbf{L}^{\perp}$. The colors appear as same as those in Fig. 2. (For interpretation of the references to color in this figure legend, the reader is referred to the web version of this article.)

can be seen, the increase in the charge density θ produces a decrease in lamellar period. This can be attributed to the fact that the B- and B'-blocks are strongly associated at larger charge density. As the phase transition from $\mathbf{L}^{||}$ to $\mathbf{L}^{\perp}$ occurs, the lamellar period of large-length-scale lamellae shows an increase. This discontinuous variation of lamellar periods implies that the phase transition is first-order. For the $\mathbf{L}^{||}$, both the periods of large-length-scale lamellae and B/B'-domains decrease. While for the $\mathbf{L}^{\perp}$, the period of large-length-scale lamellae shows a slight change and the period of small-length-scale lamellae dramatically decreases. This indicates that the A- and C-blocks become restricted to a narrower space along the normal direction as the association of B- and B'-blocks increases.

Fig. 6 illustrates the effect of charge density θ on the order parameter profiles $\phi_B(x)$-$\phi_{B'}(x)$ of the parallel lamellae-in-lamellae $\mathbf{L}^{||}$ and perpendicular lamellae-in-lamellae $\mathbf{L}^{\perp}$. (Note that $|\phi_B(x)$-$\phi_{B'}(x)| = 0$ and 1 represents that the B- and B'-blocks are disorder and complete separation, respectively.) As can be seen from Fig. 6, the values of θ have a pronounced influence on the order parameter profiles. As shown in Fig. 6a and b, with increasing the θ values, the order parameter profiles for both the hierarchical lamellae-in-lamellae show a shift to zero. This suggests that the increase in θ

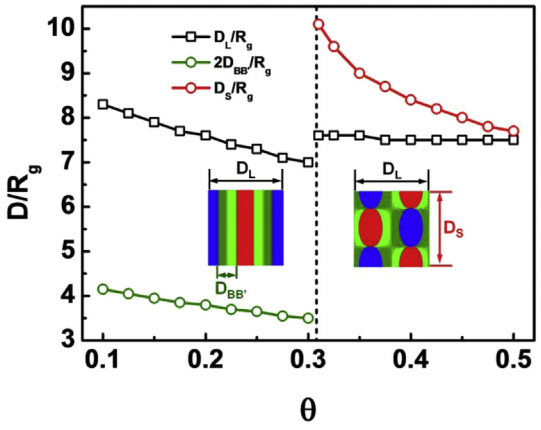

Fig. 5. Lamellar period D/R_g of $\mathbf{L}^{\|}$ and $\mathbf{L}^{\perp}$ as a function of θ for the supramolecular blends of AB- and B'C-diblock copolymers with $\chi_{BB'}N = 5$, $\gamma = 0.01$, and $\lambda = 0.1$. The large-length-scale lamellar period D_L of $\mathbf{L}^{\|}$ and $\mathbf{L}^{\perp}$, the period of BB'-domains $D_{BB'}$ of $\mathbf{L}^{\|}$ and the small-length-scale lamellar period D_S of $\mathbf{L}^{\perp}$ are schematically presented in the insets, where the D_S of $\mathbf{L}^{\|}$ is equal to $2D_{BB'}$. The colors appear as same as those in Fig. 2. (For interpretation of the references to color in this figure legend, the reader is referred to the web version of this article.)

leads to a weaker segregation between B- and B'-blocks due to the increased association of B- and B'-blocks by hydrogen bonds. To understand such an effect, the interfacial width ($w = (d\phi_B/dx)^{-1}$ at the interface [54]) was also calculated. The results for the $\mathbf{L}^{\|}$ and $\mathbf{L}^{\perp}$ were provided in the inserts of Fig. 6a and b, respectively. It can be

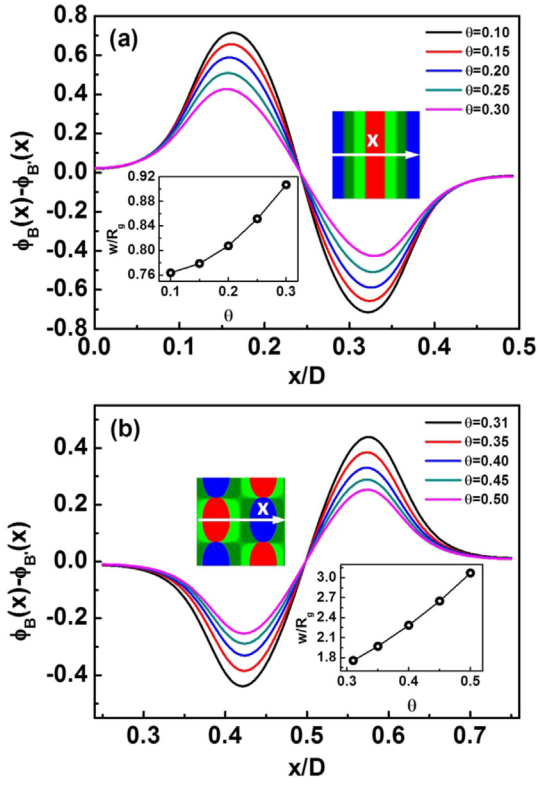

Fig. 6. Order parameter profiles $\phi_B(x) - \phi_{B'}(x)$ along the x direction of (a) $\mathbf{L}^{\|}$ and (b) $\mathbf{L}^{\perp}$ of the supramolecular blends of AB- and B'C-diblock copolymers with various values of θ. The other parameters are $\chi_{BB'}N = 5$, $\gamma = 0.01$, and $\lambda = 0.1$. D is the period of the large-length-scale lamellae. The inserts show the interfacial width and the corresponding two-dimensional lamellae where the colors appear as same as those in Fig. 2. (For interpretation of the references to color in this figure legend, the reader is referred to the web version of this article.)

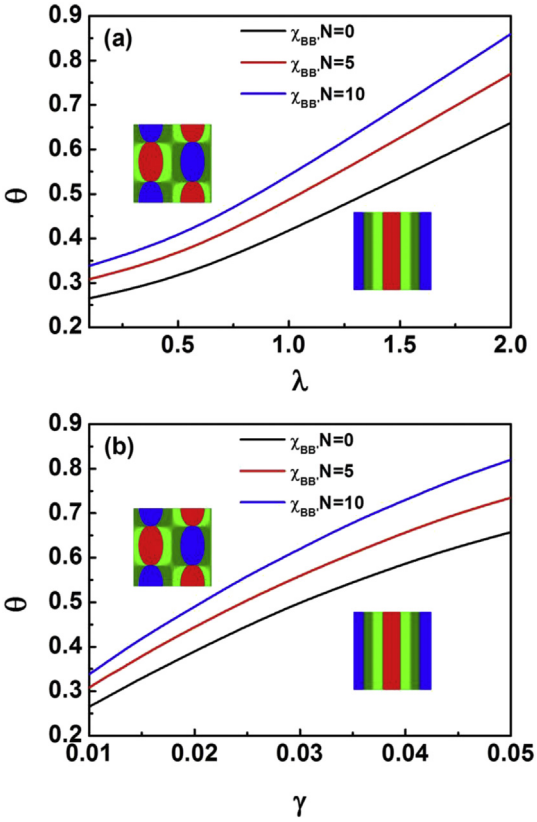

Fig. 7. Phase diagram in (a) θ–λ space at $\gamma = 0.01$ and (b) θ–γ space at $\lambda = 0.1$ for the supramolecular blends of AB- and B'C-diblock copolymers with various values of $\chi_{BB'}N$. The inserts show the two-dimensional parallel lamellae-in-lamellae $\mathbf{L}^{\|}$ and perpendicular lamellae-in-lamellae $\mathbf{L}^{\perp}$. The colors appear as same as those in Fig. 2. (For interpretation of the references to color in this figure legend, the reader is referred to the web version of this article.)

seen that the interfaces become broad as the θ increases. This also implies that the segregation between B- and B'-blocks is weaker in the blends of AB/B'C diblock copolymers with a relatively larger charge density.

Based on the obtained results, we plotted the phase diagrams in θ–λ and θ–γ spaces for the hierarchical lamellae-in-lamellae. The diagrams are shown in Fig. 7. The phase boundaries are obtained by comparing the free energies of the $\mathbf{L}^{\|}$ and $\mathbf{L}^{\perp}$. In θ–λ space, as shown in Fig. 7a, the phase boundaries from $\mathbf{L}^{\|}$ to $\mathbf{L}^{\perp}$ shift towards higher value of θ as the λ increases. In θ–γ space, as shown in Fig. 7b, the phase boundaries also show a shift to higher value of θ as the γ increases. This effect can be rationalized by considering association of B- and B'-blocks by hydrogen bonds. The increase in λ and γ corresponds to the increase of the screening effect and the decrease of the dielectric permittivity, respectively, weakening the hydrogen-bonding interaction between B- and B'-blocks. This requires more hydrogen bonds on the B- and B'-blocks to associate them together (larger θ), leading to a shift of boundaries to higher θ with increasing λ and γ.

In addition, the effect of interaction strength $\chi_{BB'}N$ between hydrogen-bonding donors and acceptors on the phase behavior of AB/B'C diblock copolymer blends was also presented in Fig. 7. In both the phase diagrams, the phase boundaries shift upwards to higher θ as $\chi_{BB'}N$ increases. This indicates that stronger hydrogen-bonding interactions are needed for the supramolecular blends with higher $\chi_{BB'}N$ to form the perpendicular lamellae-in-lamellae $\mathbf{L}^{\perp}$. An increase in the value of $\chi_{BB'}N$ ($\geq$0) can weaken the association of B- and B'-blocks. To compensate this effect, the hydrogen-

bonding interactions have to be increased, for example, increasing the density θ of hydrogen bonds on the B- and B'-blocks. This is the reason that the phase boundaries shows a shift upwards to higher θ with increasing $\chi_{BB'}N$.

3.2. Energy analysis of parallel-to-perpendicular lamellae-in-lamellae transition

To further understand the effect of hydrogen-bonding interaction on the structures, we calculated the interfacial energy U_χ/nk_BT, electrostatic energy U_e/nk_BT, and entropic loss $-S/nk_B$ for the supramolecular AB- and B'C-diblock copolymer blends with various charge densities θ. Fig. 8 shows the variations of these energies as a function of θ, where the black dot line at $\theta = 0.308$ indicates the boundary of parallel-to-perpendicular lamellae transition. As the θ increases, *i.e.*, as the hydrogen-bonding interaction increases, both the interfacial energy U_χ/nk_BT and entropy loss $-S/nk_B$ increases, and the electrostatic energy U_e/nk_BT decreases slightly. Upon phase transition from the $\mathbf{L}^{\parallel}$ to $\mathbf{L}^{\perp}$, the interfacial energy and entropic loss show a dramatic increase, and the electrostatic energy shows an abrupt decrease.

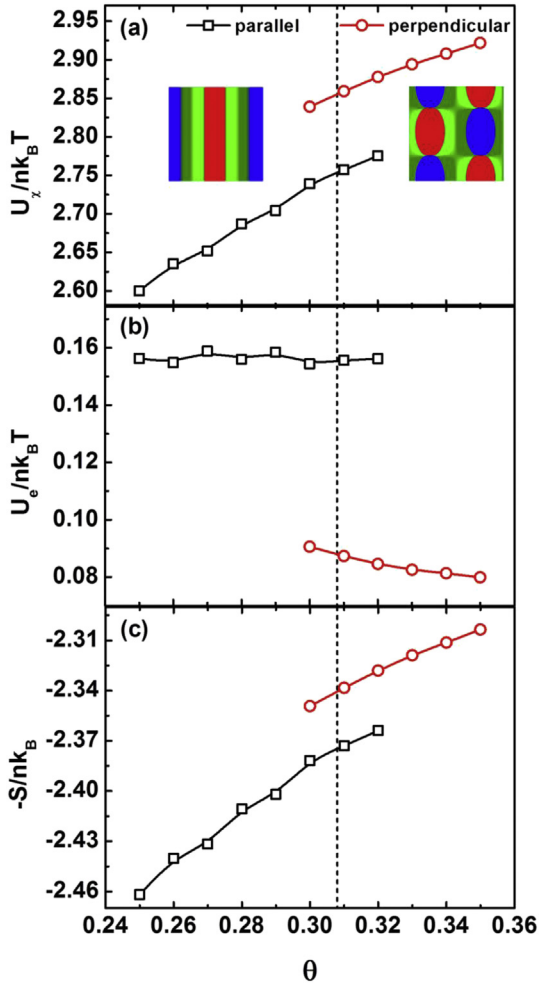

Fig. 8. Plots of (a) interfacial energy U_χ/nk_BT, (b) electrostatic energy U_e/nk_BT, and (c) entropic loss $-S/nk_B$ as a function of θ for the supramolecular AB- and B'C-diblock copolymer blends with $\chi_{BB'}N = 5$, $\gamma = 0.01$, and $\lambda = 0.1$ ($n = \rho_0 V/N$). The inserts show two-dimensional density profiles of hierarchical parallel lamellae-in-lamellae $\mathbf{L}^{\parallel}$ and hierarchical perpendicular lamellae-in-lamellae $\mathbf{L}^{\perp}$. The colors appear as same as those in Fig. 2. (For interpretation of the references to color in this figure legend, the reader is referred to the web version of this article.)

In according to the above free energy analyses, we provided a scheme to illustrate the phase transitions. The scheme is presented in Fig. 9, in which possible conformations of the supramolecular copolymers in various structures are illustrated. Combining the scheme with the energy variations (see Fig. 8), the phenomenon that the $\mathbf{L}^{\parallel}$ transforms to $\mathbf{L}^{\perp}$ with increasing the hydrogen-bonding interactions can be explained as follows. At lower hydrogen-bonding interactions, the supramolecular blends are phase-separated into $\mathbf{L}^{\parallel}$ with large period. In this way, the interfacial energy and entropic loss is minimized (Fig. 8a and c), since the specific area of A/B(B′) and C/B(B′) interfaces can be effectively reduced. With increasing the hydrogen-bonding interactions, the electrostatic energy favors the mixing of B- and B'-blocks, and the B- and B'-blocks become more associated (Fig. 9a and b). The association of B- and B'-blocks weakens the segregations of B- and B'-blocks, narrowing the lamellar period. The specific area of A/B(B′) and C/B(B′) interfaces increases, and the interfacial energy and entropic loss also increases (Fig. 8a and c). Thus, this is a process balanced by increasing electrostatic attraction and sacrificing the conformational entropy and interfacial energy.

When the interfacial energy increases to the critical point, the free energy cannot be minimized in $\mathbf{L}^{\parallel}$, and then the $\mathbf{L}^{\perp}$ is favored. Compared with Fig. 9b and c, we can see that there are more B/B′ interfaces for forming hydrogen bonds in the $\mathbf{L}^{\perp}$, as indicated by the white regions. (Note that in the $\mathbf{L}^{\parallel}$ the hydrogen bonds are formed at the B/B′ interfaces parallel to large-length-scale lamellae, while in the $\mathbf{L}^{\perp}$ the hydrogen bonds can be formed at the B/B′ interfaces not only parallel but also perpendicular to large-length-scale lamellae). As a result, the electrostatic energy decreases (Fig. 8b). However, the additional A/C interfaces is produced in the $\mathbf{L}^{\perp}$, leading to an increase in the interfacial energy (Fig. 8a). For the $\mathbf{L}^{\perp}$ at relatively lower hydrogen-bonding interactions, the period of small-length-scale lamellae is larger. This is favored by conformational entropy due to broad distribution of the blocks (Figs. 8c and 9c). As hydrogen-bonding interactions increases, the chain distribution is restricted to a narrower space owing to the increased attraction between B- and B'-blocks (Fig. 9d), and the conformational entropic loss increases (Fig. 8c). Consequently, the period of small-length-scale lamellae decreases as the hydrogen-bonding interactions increases (Fig. 5). Overall, the transition from $\mathbf{L}^{\parallel}$ to $\mathbf{L}^{\perp}$ and the decrease in their respective period are attributed to the optimization of electrostatic energy with sacrificing the entropy and interfacial energy.

3.3. Comparison with experimental observations

Some experimental findings are available in the literature for supporting our simulation results. Supramolecular blends of AB-diblock copolymers and B'-homopolymers where the B and B′ can form hydrogen bonds are the special AB/B'C supramolecular blends where the length of C-blocks vanishes. There are lots of studies on AB/B′ blend systems. For example, Chen et al. investigated the phase behavior of poly(4-vinylphenol-*b*-styrene) (PVPh-*b*-PS) blended with poly(4-vinylpyridine) (P4VP), poly(methyl methacrylate) (PMMA), and PVPh, respectively [16]. (Note that the hydrogen-bonding strength of the blend systems is in a sequence of PVPh-*b*-PS/P4VP > PVPh-*b*-PS/PMMA > PVPh-*b*-PS/PVPh.) They found a nearly linear growth of the lamellar period with the concentration of PVPh-homopolymers in the PVPh-*b*-PS/PVPh blend systems. While in the PVPh-*b*-PS/PMMA and PVPh-*b*-PS/P4VP blend systems, the lamellar spacing shows a decrease as the homopolymer concentration increases.

To reproduce such behaviors, we carried out additional calculations for the lamellar spacing of AB/B′ supramolecular blends. Fig. 10 shows the obtained normalized lamellar spacing for the

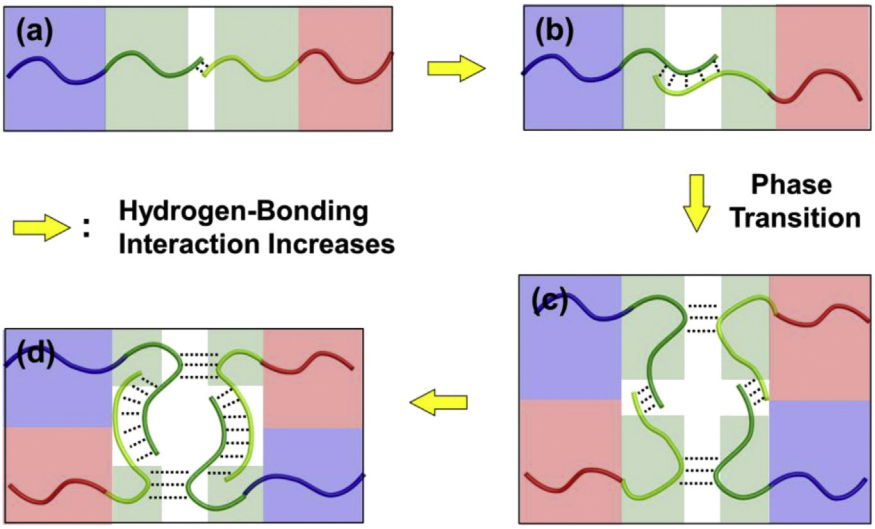

Fig. 9. Sketch of possible conformation of supramolecular copolymers in various structures, where the hydrogen-bonding interactions increase along the arrows. White regions indicate the possible interfaces for forming hydrogen bonds.

symmetric AB/B′ blend systems. The parameters were set as those in the work of Dehghan and Shi [37]. The block lengths are $N_A = N_B = N_{B'}$, and the interaction strengths are $\chi_{AB}N = 12$, $\chi_{AB'}N = 15$, and $\chi_{BB'}N = 2$. In addition, $\gamma = 0.01$ and $\lambda = 0.1$. The densities of the hydrogen-bonding accepters and donors are fixed as $\theta = \theta_B = \theta_{B'}$. As shown in Fig. 10, at the weak hydrogen-bonding regime ($\theta = 0.05$), the lamellar spacing D/D_0 increases as the concentration of B'-homopolymers increases. While at the strong hydrogen-bonding regimes ($\theta = 0.25$ and $\theta = 0.5$), the increase in homopolymer concentration results in a decrease in the lamellar spacing. These results are consistent with the experimental findings and those predicted by the interpolymer-complexation models [16,37]. This further verifies that our method is an appropriate approach to study the phase behaviors of the polymer blends with hydrogen-bonding interactions.

In addition, the revealed mechanism for the $\mathbf{L}^{\parallel}$-to-$\mathbf{L}^{\perp}$ transition could account for some experimental phenomena that need to be further clarified. Fredrickson et al. prepared blends of PEO-*b*-PS4HS (AB) and PS4VP-*b*-PMMA (B'C) with various fractions of hydrogen-bonded phenolic and pyridyl units [9,10]. As the number of hydrogen-bonding donors in PEO-*b*-PS4HS (AB) copolymers

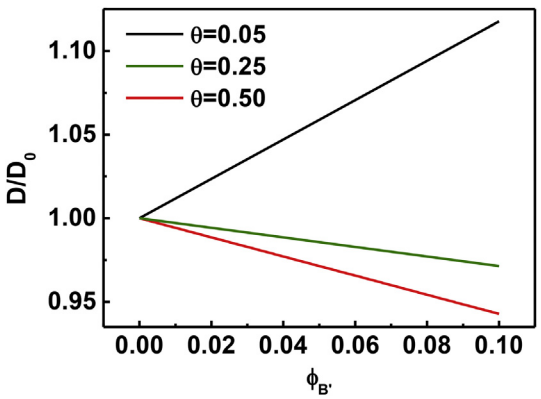

Fig. 10. Normalized lamellar spacing D/D_0 for the symmetric AB/B′ blend systems at various densities $\theta = \theta_B = \theta_{B'}$ of hydrogen-bonding acceptors and donors. The other parameters are $N_A = N_B = N_{B'}$, $\chi_{AB'}N = 12$, $\chi_{AB'}N = 15$, $\chi_{BB'}N = 2$, $\gamma = 0.01$, and $\lambda = 0.1$. D_0 is the lamellar spacing for the AB-copolymers.

increases (the number of hydrogen-bonding acceptors in PS4VP-*b*-PMMA (B'C) copolymers are fixed), the structures formed by the blends are transformed from tetragonal cylinders (Fig. 11a) to hexagonal cylinders (Fig. 11b) (both Fig. 11a and b are reproduced from ref. 10 with permission of ACS). In tetragonal cylinders (Fig. 11a), the A-cylinders are packed in a tetragonal lattice with $\mathbf{C_4}$ symmetry and distributed uniformly around the C-cylinders. In hexagonal cylinders (Fig. 11b), A- and C-blocks are intermixed to form cylinders with $\mathbf{C_6}$ symmetry. Fredrickson et al. provided an indefinite explanation for the phase transitions with donor-acceptor stoichiometry, which is as follows. Because of the excessive phenolic groups (hydrogen-bonding donors) on B-blocks, the B-blocks can interact with A- and C-blocks by hydrogen bonds. The increased interaction between B-blocks and A/C-blocks drives the phase transition from tetragonal to hexagonal cylinders.

Our work could provide an explanation for the tetragonal-to-hexagonal cylinder transition in another way. In the work carried out by Fredrickson et al., the increase in the number of hydrogen-bonding donors leads to the increase of hydrogen-bonding interactions between B- and B′ blocks. (Note that although the hydrogen bonding involves functional groups at localized sites that saturate upon bonding, the hydrogen bonding cannot reach 100% due to the entropic reason of the copolymers.) According to this experimental evidence and the mechanism revealed for the $\mathbf{L}^{\parallel}$-to-$\mathbf{L}^{\perp}$ transition, it can be deduced that the phase transition from tetragonal cylinders to hexagonal cylinders is mainly caused by the increase in hydrogen-bonding interactions. The deduction is based upon following consideration. In the hexagonal structures, the B- and B'-blocks are uniformly mixed since A- and C-blocks are mixed in the cylinders. Compared with the hexagonal structures, the B- and B'-blocks cannot be effectively mixed in the tetragonal structures with separated A- and C-cylinders. This is because the B- and B'-blocks are respectively chemically bonded to A and C-blocks, the B- and B'-blocks have to stretch themselves to mix themselves homogeneously as the A- and C-cylinders are separated. Due to enhanced mixing of B- and B'-blocks, as the tetragonal-to-hexagonal cylindrical transition occurs, both the interfacial energy and entropic loss increase. To compensate these two unfavorable energies and lower total free energy, the electrostatic energy has to decrease dramatically. As a result, only the supramolecular block copolymer systems with stronger hydrogen-

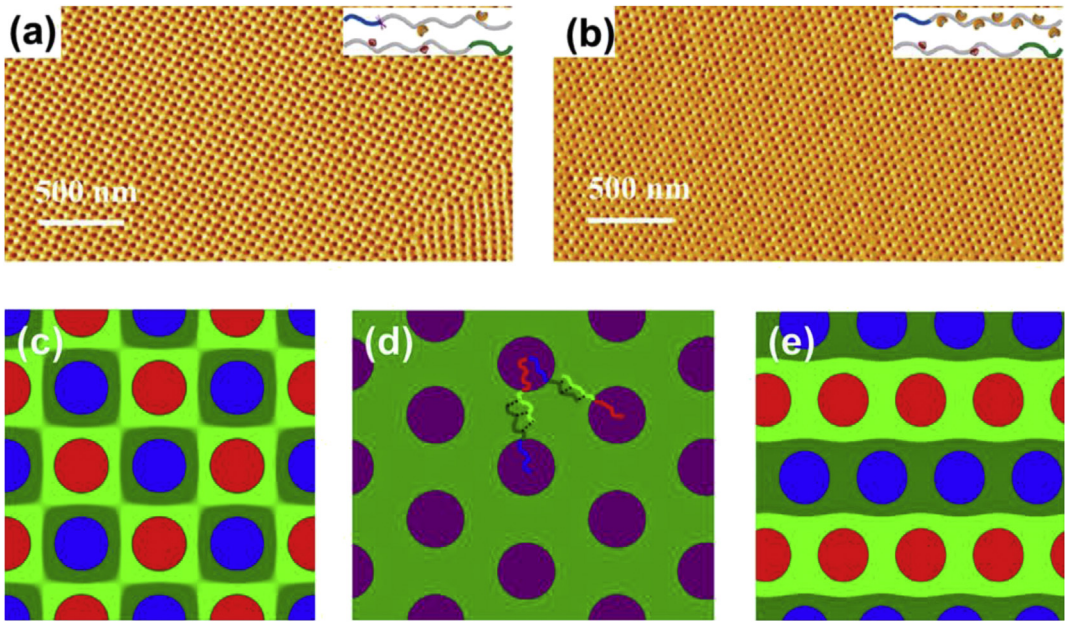

Fig. 11. SFM phase images of solvent annealed films from supramolecular block copolymer blends of PS4VP-*b*-PMMA/PEO-*b*-PS4HS (reproduced from ref. 10 with permission of ACS) for (a) tetragonal packing with $\mathbf{C_4}$ symmetry and (b) hexagonal packing with PEO and PMMA mixed. Hierarchical cylindrical microstructures self-assembled from the supramolecular blends of AB- and B'C-diblock copolymers with $f_A = f_C = 0.3$, $f_B = f_{B'} = 0.7$, $\chi_{AB}N = \chi_{AB'}N = \chi_{BC}N = \chi_{B'C}N = 20$, $\chi_{AC}N = 10$, $\chi_{BB'}N = 5$, $\gamma = 0.01$, and $\lambda = 0.1$: (c) tetragonal packing with $\mathbf{C_4}$ symmetry ($\theta = 0.05$), (d) hexagonal packing with A- and C-blocks mixed ($\theta = 0.30$), and (e) hexagonal packing with separated A- and C-cylinders (θ=0.10). The colors in the cross sections in (c) and (e) appear as same as those in Fig. 2. In (d), the polymers are schematically shown, and the purple and dark green colors are assigned to mixed AC- and BB'-domains, respectively. (For interpretation of the references to color in this figure legend, the reader is referred to the web version of this article.)

bonding interactions can meet the demand.

Based on the above analysis, we can predict that an increase in the hydrogen-bonding interactions (increase θ or decrease λ/γ) could lead to a phase transition from tetragonal to hexagonal cylinders. To test the prediction, we carried out an additional calculation for the supramolecular blends of asymmetric diblock copolymers. The lengths of AB and B'C-block copolymers were set equal and the compositions of A- and C-blocks were set as $f_A = f_C = 0.3$, according to the work of Fredrickson et al. Without the loss of generality, the other parameters are set as $\chi_{AB}N = \chi_{AB'}N = \chi_{BC}N = \chi_{B'C}N = 20$, $\chi_{AC}N = 10$, $\chi_{BB'}N = 5$, $\gamma = 0.01$, and $\lambda = 0.1$. The obtained results are shown in Fig. 10c–e. As shown in the Fig. 10c, the supramolecular blends self-assemble into tetragonal structures with separated A- and C-cylinders at $\theta = 0.05$. At higher value of θ, for example, $\theta = 0.30$, the hexagonal structures with mixed AC-cylinders is formed (Fig. 11d). The result well proves the prediction, and therefore our explanation for the phase transition can support the experimental phenomena. In addition, we found a new structure — hexagonal packing structure with separated A- and C-cylinders (Fig. 11e) — that has not been observed yet in the experiments and other SCFT calculations [10]. The formation of this type of structures is also driven by the hydrogen-bonding interactions.

The agreement with experimental observations demonstrates that the present method is capable of studying the supramolecular blends with hydrogen-bonding interactions. Although this method was originally developed for the polyelectrolytes in salt solutions [44], it also shows great power in studying polymer systems with hydrogen-bonding interactions. In contrast with the present method, the commonly used methods may not well reproduce the experimental observations of Fredrickson et al. [9,10,37–41] The difficulty in reproducing these experimental findings by the commonly used methods may be as follows. Since our work revealed that the interfacial energy exhibit marked influence on the tetragonal-to-hexagonal cylindrical transition, the treatment of hydrogen-bonding interaction with negative Flory–Huggins parameters may underestimate this important interaction [10]. As a results, the method that treats the hydrogen-bonding interactions as negative Flory–Huggins parameters could not produce these experimental observations. In addition, the present method can reproduce some other behaviors that the method with negative Flory–Huggins parameters cannot well address. For example, the method with negative Flory–Huggins parameters cannot properly describe the change of lamellar spacing induced by the addition of the B'-homopolymers to AB-diblock copolymers [37], while our method can do it (see Fig. 10). On the other hand, the hydrogen-bonding interaction, associated with the density and strength of hydrogen bonds, plays a decisive role in determining the phase transitions. Therefore, it is crucial to model the hydrogen-bonding interactions appropriately (in particular the multiple hydrogen bonds on each block). However, for the method that treats hydrogen-bonding donors/acceptors as reactive polymers [37–41], it is a rather hard task to tackle the blocks with multiple hydrogen bonds. The present work provides a new SCFT method that overcomes these two drawbacks and can be further extended other supramolecular systems with complicated hydrogen-bonding interactions.

Finally, it should be noted that saturation effect is an important property of the hydrogen bonding. However, this effect is lacking in this method because the Yukawa potential is a pair-wise potential. Some other features of the hydrogen bonds such as directional are also lacking due to the technical limitation of the SCFT. Nevertheless, it is demonstrated by comparing with available experimental and theoretical results that the hydrogen bonding of polymers could be simulated well by the present method with Yukawa potential.

4. Conclusions

A self-consistent field theory was used for studying the

supramolecular self-assembly of AB- and B'C-diblock copolymer blends with hydrogen-bonding interactions between B- and B'-blocks. The hydrogen-bonding interactions were described by the Yukawa potential, and the hydrogen-bonding donors and acceptors were modelled as B- and B'-blocks smeared with opposite screened charges. Parallel lamellae-in-lamellae and perpendicular lamellae-in-lamellae were observed. Through comparing with the free energies, phase diagrams were mapped out. The perpendicular lamellae-in-lamellae were found to be stable for the supramolecular blends with strong hydrogen-bonding interactions that are associated with higher charge density, smaller screening length, or smaller inverse amplitude of Yukawa potentials. The analyses of enthalpy and entropy reveal that the formation of perpendicular lamellae-in-lamellae at strong hydrogen-bonding interactions is favored by electrostatic energy. The obtained results can provide a reasonable explanation for the tetragonal-to-hexagonal cylinder transitions observed in the experiments for which the mechanism is not well-understood yet. The present SCFT method can be readily applied to other supramolecular blends with more complicated hydrogen-bonding interactions.

Acknowledgments

This work was supported by National Natural Science Foundation of China (21304035, 21234002, 21474029), Key Grant Project of Ministry of Education (313020), National Basic Research Program of China (No. 2012CB933600), Fundamental Research Funds for the Central Universities (222201314024), and Research Fund for the Doctoral Program of Higher Education of China (20120074120002). Support from project of Shanghai Municipality (13JC1402001) is also appreciated.

References

[1] F. Zeng, Y. Han, Z. Yan, C. Liu, C. Chen, Supramolecular polymer gel with multi stimuli responsive, self-healing and erasable properties generated by host–guest interactions, Polymer 54 (2013) 6929–6935.
[2] M. Hetzer, C. Fleischmann, B.V.K.J. Schmidt, C. Barner-Kowollik, H. Ritter, Visual recognition of supramolecular graft polymer formation via phenolphthalein–cyclodextrin association, Polymer 54 (2013) 5141–5147.
[3] A. Noro, K. Ishihara, Y. Matsushita, Nanophase-separated supramolecular assemblies of two functionalized polymers via acid-base complexation, Macromolecules 44 (2011) 6241–6244.
[4] K. Dobrosielska, S. Wakao, A. Takano, Y. Matsushita, Nanophase-separated structures of AB block copolymer/C homopolymer blends with complementary hydrogen-bonding interactions, Macromolecules 41 (2008) 7695–7698.
[5] N. Houbenov, A. Nykänen, H. Iatrou, N. Hadjichristidis, J. Ruokolainen, C. Faul, O. Ikkala, Fibrillar constructs from multilevel hierarchical self-assembly of discotic and calamitic supramolecular motifs, Adv. Funct. Mater. 18 (2008) 2041–2047.
[6] T. Aida, E.W. Meijer, S.I. Stupp, Functional supramolecular polymers, Science 335 (2012) 813–817.
[7] J. Ruokolainen, R. Mäkinen, M. Torkkeli, T. Mäkelä, T. Serimaa, G. ten Brinke, O. Ikkala, Switching supramolecular polymeric materials with multiple length scales, Science 280 (1998) 557–560.
[8] T. Asari, S. Matsuo, A. Takano, Y. Matsushita, Three-phase hierarchical structures from AB/CD diblock copolymer blends with complemental hydrogen bonding interaction, Macromolecules 38 (2005) 8811–8815.
[9] C. Tang, E.M. Lennon, G.H. Fredrickson, E.J. Kramer, C.J. Hawker, Evolution of block copolymer lithography to highly ordered square arrays, Science 322 (2008) 429–432.
[10] C. Tang, S. Hur, B.C. Stahl, K. Sivanandan, M. Dimitriou, E. Pressly, G.H. Fredrickson, E.J. Kramer, C.J. Hawker, Thin film morphology of block copolymer blends with tunable supramolecular interactions for lithographic applications, Macromolecules 43 (2010) 2880–2889.
[11] S. Shinde, S.K. Asha, Self-assembly directed template photopolymerization of perylenebisimide-poly(4-vinylpyridine): nano organization, Polymer 65 (2015) 115–123.
[12] S. Sami, E. Yildirim, M. Yurtsever, E. Yurtsever, E. Yilgor, I. Yilgor, G.L. Wilkes, Understanding the influence of hydrogen bonding and diisocyanate symmetry on the morphology and properties of segmented polyurethanes and polyureas: computational and experimental study, Polymer 55 (2014) 4563–4576.
[13] S. Ma, X. Qi, Y. Cao, S. Yang, J. Xu, Hydrogen bond detachment in polymer complexes, Polymer 54 (2013) 5382–5390.
[14] G. Song, Y. Zhang, D. Wang, C. Chen, H. Zhou, X. Zhao, G. Dang, Intermolecular interactions of polyimides containing benzimidazole and benzoxazole moieties, Polymer 54 (2013) 2335–2340.
[15] D. Tsiourvas, M. Arkas, Columnar and smectic self-assembly deriving from non ionic amphiphilic hyperbranched polyethylene imine polymers and induced by hydrogen bonding and segregation into polar and non polar parts, Polymer 54 (2013) 1114–1122.
[16] S.-C. Chen, S.-W. Kuo, U.-S. Jeng, C.-J. Su, F.-C. Chang, On modulating the phase behavior of block copolymer/homopolymer blends via hydrogen bonding, Macromolecules 43 (2010) 1083–1092.
[17] F. Tanaka, M. Ishida, A. Matsuyama, Theory of microphase formation in reversibly associating block copolymer blends, Macromolecules 24 (1991) 5582–5589.
[18] H.J. Angerman, G. ten Brinke, Weak segregation theory of microphase separation in associating binary homopolymer blends, Macromolecules 32 (1999) 6813–6820.
[19] J. Huh, W.H. Jo, Theory on phase behavior of triblocklike supramolecules formed from reversibly associating end-functionalized polymer blends, Macromolecules 37 (2004) 3037–3048.
[20] Y. Han, W. Jiang, Self-assembly of the AB/BC diblock copolymer mixture based on hydrogen bonding in a selective solvent: a Monte Carlo study, J. Phys. Chem. B 115 (2011) 2167–2172.
[21] G. Quan, M. Wang, C. Tong, A numerical study of spherical polyelectrolyte brushes by the self-consistent field theory, Polymer 55 (2014) 6604–6613.
[22] C.L. Ting, Z.-G. Wang, Minimum free energy paths for a nanoparticle crossing the lipid membrane, Soft Matter 8 (2012) 12066–12071.
[23] X. Ye, T. Shi, Z. Lu, C. Zhang, Z. Sun, L. An, Study of morphology and phase diagram of π-shaped ABC block copolymers using self-consistent-field theory, Macromolecules 38 (2005) 8853–8857.
[24] G. Quan, Y. Zhu, C. Tong, The numerical study of the adsorption of bi-disperse flexible polyelectrolytes onto the surface of two charged objects, Polymer 54 (2013) 6834–6842.
[25] X. Wang, M. Goswami, R. Kumar, B.G. Sumpter, J. Mays, Morphologies of block copolymers composed of charged and neutral blocks, Soft Matter 8 (2012) 3036–3051.
[26] Y. Xia, Z. Sun, T. Shi, J. Chen, L. An, Y. Jia, Self-assembly of rod-terminally tethered three-armed star-shaped coil block copolymer: investigation of the presence of the branching in the coil to the self-assembled behavior, Polymer 49 (2008) 5596–5601.
[27] Y. Xia, J. Chen, Z. Sun, T. Shi, L. An, Y. Jia, Self-assembly of linear ABC coil–coil–rod triblock copolymers, Polymer 51 (2010) 3315–3319.
[28] L. Wang, J. Lin, Discovering multicore micelles: insights into the self-assembly of linear ABC terpolymers in midblock-selective solvents, Soft Matter 7 (2011) 3383–3391.
[29] Y. Zhuang, L. Wang, J. Lin, L. Zhang, Phase behavior of graft copolymers in concentrated solution, Soft Matter 7 (2011) 137–146.
[30] X. Ye, B.J. Edwards, B. Khomami, Block copolymer morphology formation on topographically complex surfaces: a self-consistent field theoretical study, Macromol. Rapid Commun. 35 (2014) 702–707.
[31] X. Ye, X. Yu, T. Shi, Z. Sun, L. An, Z. Tong, A self-consistent field theory study on the morphologies of linear ABCBA and H-shaped $(AB)_2C(BA)_2$ block copolymers, J. Phys. Chem. B 110 (2006) 23578–23582.
[32] D. Sun, Z. Sun, H. Li, L. An, Study of morphology and phase diagram of the H-shaped (AC)B(CA) ternary block copolymers using self-consistent field theory, Polymer 50 (2009) 4270–4280.
[33] D. Sun, Z. Sun, H. Li, L. An, Effects of asymmetric interaction energies on the micro-phase separation behavior of H-shaped (AC)B(CA) ternary block copolymer systems: a real space self-consistent field theory study, Macromol. Theory Simul. 19 (2010) 100–112.
[34] X. Cao, L. Zhang, L. Wang, J. Lin, Insights into ordered microstructures and ordering mechanisms of ABC star terpolymers by integrating dynamic self-consistent field theory and variable cell shape methods, Soft Matter 10 (2014) 5916–5927.
[35] R. Wang, Z. Jiang, H. Yang, G. Xue, Side chain effect on the self-assembly of coil-comb copolymer by self-consistent field theory in two dimensions, Polymer 54 (2013) 7080–7087.
[36] Y.-C. Hsu, C.-I. Huang, W. Li, F. Qiu, A.-C. Shi, Micellization of Linear A-*b*-(B-*alt*-C)$_n$ multiblock terpolymers in A-selective solvents, Polymer 54 (2013) 431–439.
[37] A. Dehghan, A.-C. Shi, Modeling hydrogen bonding in diblock copolymer/homopolymer blends, Macromolecules 46 (2013) 5796–5805.
[38] X. Zhang, L. Wang, T. Jiang, J. Lin, Phase behaviors of supramolecular graft copolymers with reversible bonding, J. Chem. Phys. 139 (2013) 184901–184912.
[39] Y. Zhuang, L. Wang, J. Lin, Hierarchical nanostructures self-assembled from diblock copolymer/homopolymer blends with supramolecular interactions, J. Phys. Chem. B 115 (2011) 7550–7560.
[40] E.H. Feng, W.B. Lee, G.H. Fredrickson, Supramolecular diblock copolymers: a field-theoretic model and mean-field solution, Macromolecules 40 (2007) 693–702.
[41] W.B. Lee, R. Elliott, K. Katsov, G.H. Fredrickson, Phase morphologies in reversibly bonding supramolecular triblock copolymer blends, Macromolecules 40 (2007) 8445–8454.
[42] P.U. Kenkare, C.K. Hall, Modeling of phase separation in PEG-salt aqueous

two-phase systems, AIChE J. 42 (1996) 3508–3522.
[43] P. Koehl, H. Orland, M. Delarue, Beyond the Poisson–Boltzmann model: modeling biomolecule–water and water–water Interactions, Phys. Rev. Lett. 102 (2009) 087801–087804.
[44] E.A. Nogovitsin, Y.A. Budkov, Self-consistent field theory investigation of the behavior of hyaluronic acid chains in aqueous salt solutions, Phys. A 391 (2012) 2507–2517.
[45] G.H. Fredrickson, The Equilibrium Theory of Inhomogeneous Polymers, Oxford University Press, Oxford, U.K., 2006.
[46] F. Drolet, G.H. Fredrickson, Optimizing chain bridging in complex block copolymers, Macromolecules 34 (2001) 5317–5324.
[47] F. Drolet, G.H. Fredrickson, Combinatorial screening of complex block copolymer assembly with self-consistent field theory, Phys. Rev. Lett. 83 (1999) 4317–4320.
[48] V. Ganesan, G.H. Fredrickson, Field-theoretic polymer simulations, Europhys. Lett. 55 (2001) 814–820.
[49] FFTW, http//www/fftw.org/.
[50] J.U. Kim, M.W. Matsen, Droplets of structured fluid on a flat substrate, Soft Matter 5 (2009) 2889–2895.
[51] L. Wang, J. Lin, Q. Zhang, Self-consistent field theory study of the solvation effect in polyelectrolyte solutions: beyond the Poisson–Boltzmann model, Soft Matter 9 (2013) 4015–4025.
[52] Y. Bohbot-Raviv, Z.-G. Wang, Discovering new ordered phases of block copolymers, Phys. Rev. Lett. 85 (2000) 3428–3431.
[53] W.-C. Chen, S.-W. Kuo, F.-C. Chang, Self-assembly of an A–B diblock copolymer blended with a C homopolymer and a C–D diblock copolymer through hydrogen bonding interaction, Polymer 51 (2010) 4176–4184.
[54] M.W. Matsen, R.B. Thompson, Equilibrium behavior of symmetric ABA triblock copolymer melts, J. Chem. Phys. 111 (1999) 7139–7146.